Prediction of Post-Cure Residual Stresses and Distortions in the Fabrication of Composite Structures

A. R. de Faria[*], M. Åkermo[**], S. Hallström[**], T. Nyman[***], F. Ferraz[****]

[*]Department of Mechanical Engineering, Instituto Tecnológico de Aeronáutica - ITA, São José dos Campos, SP, Brazil (E-mail: *arfaria@ita.br*)

[**]Royal Institute of Technology (KTH), Dept. of Aeronautical and Vehicle Engineering, Teknikringen 8, SE 100 44 Stockholm, Sweden (E-mail: *akermo@kth.se; stefanha@kth.se*)

[***]SAAB Aerostructures, Linköping, Sweden (E-mail: *tonny.nyman@saabgroup.com*)

[****]AKAER Aerostructures, São José dos Campos, SP, Brazil (E-mail: *fernando.ferraz@akaer.com.br*)

Abstract: Distortions and residual stresses are inherently present in advanced composite structures that undergo curing cycles at elevated temperature. These are undesirable effects of the fabrication processes since distortions deviate the structure from the nominal geometry, what can compromise aerodynamic performance or make impossible assemblage of structural components. Residual stresses are the driving mechanisms to induced distortions but, additionally, they may significantly and adversely reduce the strength of composite structures. In this work a model intended to predict the levels of distortions and residual stresses shall be developed and embedded in an in-house FE code. The model shall take into account thermal, chemical and frozen-in strains that develop during curing cycles.

Keywords: Manufacturing distortions, Residual stresses, Cure kinetics, Numerical simulation, Finite elements.

INTRODUCTION

The necessity to understand the consolidation and cure fabrication processes of themoset composites motivated a number of studies (Lundström 1993, Kenny *et al.* 1990, Kenny 1992). However, constitutive models specifically tailored to model resin cure and residual stress development are relatively rare.

Thermal contraction has been shown to be an important mechanism that induces the appearance of residual stresses and distortions (Hull 1998). Spring-back effects and distortions were observed to generally increase with increasing cure temperature (Sarrazin *et al.* 1995, White *et al.* 1993). Another relevant mechanism that contributes to building up residual stresses is chemical shrinkage of the resin (White *et al.* 1993, Holmberg 1998). A third mechanism is permanent frozen deformation (Holmberg 1998, Kolkman 1974). This, however, derives from mechanical constraints imposed by the mould in RTM processes and therefore may be negligible in AFP or ATL fabrication processes.

In a series of papers Svanberg and co-workers (Svanberg *et al.* 2001, 2004a, 2004b) proposed a very pragmatic constitutive model that include thermal contraction, chemical shrinkage and frozen-in deformations. They proposed a path dependent constitutive model that requires only six stress state variables, all of them functions of the degree of cure and temperature. Viscoelastic effects were ignored since it was assumed that rate dependence is unimportant, or at least negligible in the cure of thermosets.

In addition to the three mechanism cited above others are also certainly important: unsymmetric laminates (Cho *et al.* 1998), temperature and cure gradients (Kim *et al.* 1997) and gradients in fiber volume fraction (Radford 1997). The lack of symmetric in a laminate is taken into account by the nonzero laminate B matrix that couples membrane to curvature strains. Temperature gradients can be considered through a computation as simples as the difference between room and glass transition cure temperature. More accurate predictions would require some sort of heat transfer model to obtain accurate temperature distribution during cure and subsequent cool down to room temperature. Cure gradients have to be evaluated with the aid of a state variable, the degree of cure, that usually varies from 0 (uncured) to 1 (fully cured). Gradient in the fiber volume fraction reflect in the mechanical properties of the layers and the laminate itself. These can be accounted for by the traditional micromechanical rule of mixtures approach (Kaw 2006).

The accurate of residual stresses is paramount due to their potential deleterious effects. A simple example is the change in stiffness produced by residual stresses through geometric stiffening when residual stresses couple with the nonlinear strains. It was shown that this stress stiffening can substantially affect buckling (Faria *et al.* 1999) and natural frequencies of composite structures (Almeida *et al.* 1999) fabricated by curing at elevated temperatures. Evidently strength characteristics of composite laminates are also affected by the presence of residual stresses that physically represent an initial nonzero stress state within the layers. In addition to mechanical stresses produced by the mechanical loads the structure shall be subjected during its operation, the residual stresses inherited from curing must be added in order obtain the resultant stress state used to compute the onset of failure.

Most scientific works that need to evaluate residual stresses in composite structures fabricated at high temperature cure cycles assume that the temperature gradient is simply given by the difference between the operation, or room temperature, and the glass transition temperature, neglecting aspects such as chemical shrinkage strains, the variation of the glass transition temperature with the degree of cure, and the existence of glassy and rubbery states of the resin.

The implementation of a constitutive model that is comprehensive enough to consider the aspects mentioned above will enable engineers and researchers to obtain much more precise descriptions of the residual stress distributions and to predict beforehand whether undesirable spring-back effects shall manifest after cure. It is expected that the numerical models to be developed will be useful in future projects partners in the aerospace industry. The code implemented shall be used to obtain numerical results that shall be compared against the results obtained from the material characterization and structural tests in the coupon level. If the code proves to be accurate enough it will be able to predict residual stresses, spring-back and distortions occurring in representative parts and primary structural components of real aircraft.

THEORETICAL BACKGROUND

The present section describes the thermomechanical elastic theory, the finite element formulation and numerical solution strategy used.

Thermomechanical elastic theory

The additive decomposition of the strain is assumed such that the total strain can be written as

$$\boldsymbol{\varepsilon} = \boldsymbol{\varepsilon}_e + \boldsymbol{\varepsilon}_t + \boldsymbol{\varepsilon}_c \tag{1}$$

where $\boldsymbol{\varepsilon}_e$ is the elastic part, $\boldsymbol{\varepsilon}_t$ is the thermal strain and $\boldsymbol{\varepsilon}_c$ is chemical shrinkage strains. $\boldsymbol{\varepsilon}_t$ and $\boldsymbol{\varepsilon}_c$ are given by

$$\boldsymbol{\varepsilon}_t = (T - T_0)\boldsymbol{\alpha} \qquad \boldsymbol{\varepsilon}_c = (X - X_0)\boldsymbol{\beta} \tag{2}$$

where T_0 and X_0 are reference temperature and degree of cure. The coefficients of thermal expansion ($\boldsymbol{\alpha}$) and chemical shrinkage ($\boldsymbol{\beta}$) depend on the temperature (T) and degree of cure (X) as

$$\boldsymbol{\alpha} = \begin{cases} \boldsymbol{\alpha}_l, & X < X_{gel}, \quad T \geq T_g(X) \\ \boldsymbol{\alpha}_r, & X \geq X_{gel}, \quad T \geq T_g(X) \\ \boldsymbol{\alpha}_g, & T < T_g(X) \end{cases}, \quad \boldsymbol{\beta} = \begin{cases} \boldsymbol{\beta}_l, & X < X_{gel}, \quad T \geq T_g(X) \\ \boldsymbol{\beta}_r, & X \geq X_{gel}, \quad T \geq T_g(X) \\ \boldsymbol{\beta}_g, & T < T_g(X) \end{cases} \tag{3}$$

where the subscripts 'l', 'r' and 'g' refer respectively to liquid, rubbery and glassy states. T_g is the glass transition temperature and X_{gel} denotes degree of cure at gelation. The glass transition temperature relates T_g to X by the DiBenedetto equation:

$$\frac{T_g - T_{g0}}{T_{g\infty} - T_{g0}} = \frac{\lambda X}{1 - (1 - \lambda)X} \tag{4}$$

where T_{g0} and $T_{g\infty}$ are the glass transition temperature of the uncured (X = 0) and fully cured (X = 1) resin and λ is a material constant.

Notice that Eq. (1) can be rewritten as

$$\boldsymbol{\varepsilon}_e = \boldsymbol{\varepsilon} - \boldsymbol{\varepsilon}_t - \boldsymbol{\varepsilon}_c \tag{5}$$

Mathematically there is little interest in writing Eq. (5). However, from a physical point of view, Eq. (5) can be interpreted as a way of determining the elastic strains, i.e., if the *total strain* is stripped from the thermal and chemical strains, the remaining part is the purely elastic strain. This is an important issue that comes into play when the material constitutive equation is written.

The incremental stresses can be written as

$$\Delta\boldsymbol{\sigma} = \begin{cases} \mathbf{C}_r \Delta(\boldsymbol{\varepsilon} - \boldsymbol{\varepsilon}_t - \boldsymbol{\varepsilon}_c) - \mathbf{s} & , \quad T \geq T_g(X) \\ \mathbf{C}_g \Delta(\boldsymbol{\varepsilon} - \boldsymbol{\varepsilon}_t - \boldsymbol{\varepsilon}_c) & , \quad T < T_g(X) \end{cases} \tag{6}$$

where $\mathbf{C}_r$ is the rubbery modulus tensor and $\mathbf{C}_g$ is the glassy modulus tensor. In the most general situation $\Delta\boldsymbol{\sigma}$ contains six stress components: $\Delta\sigma_{xx}$, $\Delta\sigma_{yy}$, $\Delta\sigma_{zz}$, $\Delta\tau_{yz}$, $\Delta\tau_{xz}$ and $\Delta\tau_{xy}$. Similar observation holds for $\Delta\boldsymbol{\varepsilon}$, $\Delta\boldsymbol{\varepsilon}_t$ and $\Delta\boldsymbol{\varepsilon}_c$, each one also containing six strain components. The thermal and chemical strain increments computed in Eq. (6) are $\Delta\boldsymbol{\varepsilon}_t = \boldsymbol{\alpha}\Delta T$ and $\Delta\boldsymbol{\varepsilon}_c = \beta\Delta X$.

The state variables s are

$$\mathbf{s}(t+\Delta t)=\begin{cases} 0 & , \quad T \geq T_g(X) \\ \mathbf{s}(t)+(\mathbf{C}_g-\mathbf{C}_r)\Delta(\boldsymbol{\varepsilon}-\boldsymbol{\varepsilon}_t-\boldsymbol{\varepsilon}_c) & , \quad T < T_g(X) \end{cases} \tag{7}$$

It is clear that the state variables correspond to stresses that keep track of the loading history. In the rubbery state the state variables become zero, meaning that the stress history has been erased. In the glassy state **s** represent frozen-in stresses.

Finite element formulation

Triangular and quadrilateral plate elements are shown in Fig. 1 with their respective local coordinate systems, both with the origin situated at the elements' centroids. The element orientation is determined based its edges. The *x* axis in both cases is parallel to side 1-2. Denote $\mathbf{v}_{ij}$ the unit vector in the direction from node *i* to node *j*. In the triangular element the *z* axis is defined along the direction $\mathbf{v}_{12} \times \mathbf{v}_{13}$ whereas in the quadrilateral element the *z* axis is defined along the direction $\mathbf{v}_{12} \times \mathbf{v}_{14}$. Once the axes *x* and *z* are defined the *y* axis is determined by cross product.

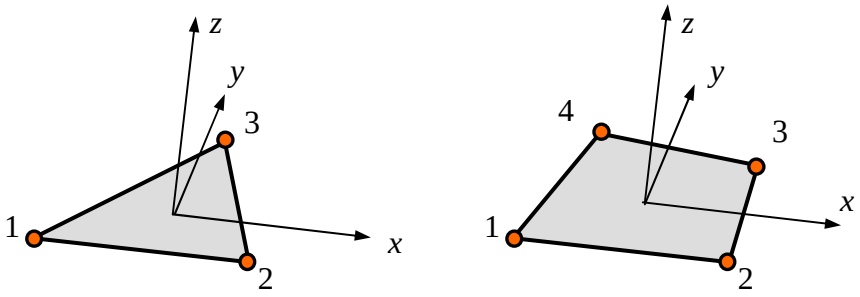

Figure 1: Triangular and quadrilateral plate elements.

The kinematic relations follow the Mindlin plate theory where displacements of an arbitrary point within the element, in the local coordinate system, are given by

$$\begin{aligned} \bar{u}(x,y,z) &= u(x,y)+z\theta_y(x,y) \\ \bar{v}(x,y,z) &= v(x,y)-z\theta_x(x,y) \\ \bar{w}(x,y,z) &= w(x,y) \end{aligned} \tag{8}$$

where displacements *u* and *v* are those measured with reference to the element mid surface. Equation (8) allows one to derive the strains:

$$\begin{aligned} &\varepsilon_{xx}=\frac{\partial u}{\partial x}+z\frac{\partial \theta_y}{\partial x} \quad , \quad \varepsilon_{yy}=\frac{\partial v}{\partial y}-z\frac{\partial \theta_x}{\partial y} \quad , \quad \varepsilon_{zz}=0 \\ &\gamma_{xy}=\frac{\partial u}{\partial y}+\frac{\partial v}{\partial x}+z\left(\frac{\partial \theta_y}{\partial y}-\frac{\partial \theta_x}{\partial x}\right) \quad , \quad \gamma_{xz}=\frac{\partial w}{\partial x}+\theta_y \quad , \quad \gamma_{yz}=\frac{\partial w}{\partial y}-\theta_x \end{aligned} \tag{9}$$

A drilling degree of freedom is not explicitly present in Eq. (9). However, for completeness, the drilling (θ_z) will also be included in the following derivations.

Discretization of the element is now performed. The displacements are interpolated according to

$$(u,v,w,\theta_x,\theta_y,\theta_z)=\sum_{i=1}^{m}\phi_i(u_i,v_i,w_i,\theta_{xi},\theta_{yi},\theta_{zi}) \tag{10}$$

where there are m nodes, ϕ_i are interpolation functions and u_i, v_i, w_i, θ_{xi}, θ_{yi} and θ_{zi} are nodal degrees of freedom. The virtual displacements are similarly interpolated, i.e.,

$$(\delta u, \delta v, \delta w, \delta\theta_x, \delta\theta_y, \delta\theta_z) = \sum_{i=1}^{m} \phi_i (\delta u_i, \delta v_i, \delta w_i, \delta\theta_{xi}, \delta\theta_{yi}, \delta\theta_{zi}) \tag{11}$$

The element vector of nodal degrees of freedom is defined as $\mathbf{q}_e = \{u_1\ v_1\ w_1\ \theta_{x1}\ \theta_{y1}\ \theta_{z1}\ \ldots\ u_m\ v_m\ w_m\ \theta_{xm}\ \theta_{ym}\ \theta_{zm}\}^T$ and its virtual counterpart is $\delta\mathbf{q}_e = \{\delta u_1\ \delta v_1\ \delta w_1\ \delta\theta_{x1}\ \delta\theta_{y1}\ \delta\theta_{z1}\ \ldots\ \delta u_m\ \delta v_m\ \delta w_m\ \delta\theta_{xm}\ \delta\theta_{ym}\ \delta\theta_{zm}\}^T$. Matrices of derivatives of the interpolation functions are defined as

$$\mathbf{B}_{mi} = \begin{bmatrix} \phi_{i,x} & 0 & 0 & 0 & 0 & 0 \\ 0 & \phi_{i,y} & 0 & 0 & 0 & 0 \\ \phi_{i,y} & \phi_{i,x} & 0 & 0 & 0 & 0 \end{bmatrix} \quad , \quad \mathbf{B}_{bi} = \begin{bmatrix} 0 & 0 & 0 & 0 & \phi_{i,x} & 0 \\ 0 & 0 & 0 & -\phi_{i,y} & 0 & 0 \\ 0 & 0 & 0 & -\phi_{i,x} & \phi_{i,y} & 0 \end{bmatrix}$$
$$\mathbf{B}_{si} = \begin{bmatrix} 0 & 0 & \phi_{i,y} & -\phi_i & 0 & 0 \\ 0 & 0 & \phi_{i,x} & 0 & \phi_i & 0 \end{bmatrix} \tag{12}$$

Equations (10) and (12) can be substituted into (9) to compute the strains within each element as

$$\boldsymbol{\varepsilon}_0 = \begin{Bmatrix} \varepsilon_{xx} \\ \varepsilon_{yy} \\ \gamma_{xy} \end{Bmatrix} = \begin{Bmatrix} u_{,x} \\ v_{,y} \\ u_{,y} + v_{,x} \end{Bmatrix} = \sum_{i=1}^{m} \mathbf{B}_{mi} \{u_i \quad v_i \quad w_i \quad \theta_{xi} \quad \theta_{yi} \quad \theta_{zi}\}^T = \mathbf{B}_m \mathbf{q}_e$$
$$\boldsymbol{\kappa} = \begin{Bmatrix} \kappa_{xx} \\ \kappa_{yy} \\ \kappa_{xy} \end{Bmatrix} = \begin{Bmatrix} \theta_{y,x} \\ -\theta_{x,y} \\ \theta_{y,y} - \theta_{x,x} \end{Bmatrix} = \sum_{i=1}^{m} \mathbf{B}_{bi} \{u_i \quad v_i \quad w_i \quad \theta_{xi} \quad \theta_{yi} \quad \theta_{zi}\}^T = \mathbf{B}_b \mathbf{q}_e$$
$$\boldsymbol{\gamma} = \begin{Bmatrix} \gamma_{yz} \\ \gamma_{xz} \end{Bmatrix} = \begin{Bmatrix} w_{,y} - \theta_x \\ w_{,x} + \theta_y \end{Bmatrix} = \sum_{i=1}^{m} \mathbf{B}_{si} \{u_i \quad v_i \quad w_i \quad \theta_{xi} \quad \theta_{yi} \quad \theta_{zi}\}^T = \mathbf{B}_s \mathbf{q}_e \tag{13}$$

where $\boldsymbol{\varepsilon}_0$, $\boldsymbol{\kappa}$, $\boldsymbol{\gamma}$ are, respectively, membrane, curvature and transverse shear strains. Notice that matrices $\mathbf{B}_m$, $\mathbf{B}_b$ and $\mathbf{B}_s$ may differ from element to element.

Accompanying the strains in Eq. (9) are the respective stresses σ_{xx}, σ_{yy}, τ_{xy}, τ_{yz} and τ_{xz}. These can be grouped in in-plane stresses (σ_{xx}, σ_{yy}, τ_{xy}) and transverse shear stresses (τ_{yz}, τ_{xz}) such that, for element e,

$$\boldsymbol{\sigma}_e = \{\sigma_{xx} \quad \sigma_{yy} \quad \tau_{xy}\}^T \quad , \quad \boldsymbol{\tau}_e = \{\tau_{yz} \quad \tau_{xz}\}^T \tag{14}$$

It is clear from Eq. (6) that the state variables $\mathbf{s}$ correspond to stresses. Thus, they can also be stored, similarly to Eq. (14), in two groups

$$\mathbf{s}_{\sigma e} = \{s_{xx} \quad s_{yy} \quad s_{xy}\}^T \quad , \quad \mathbf{s}_{\tau e} = \{s_{yz} \quad s_{xz}\}^T \tag{15}$$

Numerical solution

The principle of virtual work allows one to write

$$\sum_{e=1}^{N_e}\int_{V_e}[(\delta\boldsymbol{\varepsilon}_0^T + z\delta\boldsymbol{\kappa}^T)\boldsymbol{\sigma}_e + \delta\boldsymbol{\gamma}^T\boldsymbol{\tau}_e]dV_e = \sum_{e=1}^{N_e}\int_{V_e}\delta\mathbf{q}_e^T\mathbf{f}_e dV_e \tag{16}$$

where summation extends over all N_e elements in the mesh and $\mathbf{f}_e$ is the vector of external loads applied to element e. Substitution of Eq. (13) into (16), and recognizing that $\delta\mathbf{q}_e$ are arbitrary and geometrically admissible virtual displacements,

$$\sum_{e=1}^{N_e}\int_{V_e}[(\mathbf{B}_m^T + z\mathbf{B}_b^T)\boldsymbol{\sigma}_e + \mathbf{B}_s^T\boldsymbol{\tau}_e]dV_e = \mathbf{f}_{ext} \tag{17}$$

where the combined effects of all $\mathbf{f}_e$ have been grouped into $\mathbf{f}_{ext}$. The left-hand side of Eq. (17) is the vector of internal forces. Theoretically the problem to be solved is: given $\mathbf{f}_{ext}$ find the stresses $\boldsymbol{\sigma}_e$, $\boldsymbol{\tau}_e$ that satisfy the equilibrium condition posed by Eq. (17). This is a generally nonlinear problem whose solution is obtained incrementally.

Initially consider that the equilibrium problem has been solved for time step n such that

$$\sum_{e=1}^{N_e}\int_{V_e}[(\mathbf{B}_m^T + z\mathbf{B}_b^T)\boldsymbol{\sigma}_e^n + \mathbf{B}_s^T\boldsymbol{\tau}_e^n]dV_e = \mathbf{f}_{ext}^n \tag{18}$$

Next, increment the load at step $n + 1$ and find the new stresses that satisfy

$$\sum_{e=1}^{N_e}\int_{V_e}[(\mathbf{B}_m^T + z\mathbf{B}_b^T)(\boldsymbol{\sigma}_e^n + \Delta\boldsymbol{\sigma}_e^{n+1}) + \mathbf{B}_s^T(\boldsymbol{\tau}_e^n + \Delta\boldsymbol{\tau}_e^{n+1})]dV_e = \mathbf{f}_{ext}^{n+1} \tag{19}$$

with $\boldsymbol{\sigma}_e^{n+1} = \boldsymbol{\sigma}_e^n + \Delta\boldsymbol{\sigma}_e^{n+1}$ and $\boldsymbol{\tau}_e^{n+1} = \boldsymbol{\tau}_e^n + \Delta\boldsymbol{\tau}_e^{n+1}$. Solution of Eq. (19) must be found iteratively. Rearrangement of Eq. (19) leads to

$$\sum_{e=1}^{N_e}\int_{V_e}[(\mathbf{B}_m^T + z\mathbf{B}_b^T)\Delta\boldsymbol{\sigma}_e^{n+1} + \mathbf{B}_s^T\Delta\boldsymbol{\tau}_e^{n+1}]dV_e = \mathbf{f}_{ext}^{n+1} - \sum_{e=1}^{N_e}\int_{V_e}[(\mathbf{B}_m^T + z\mathbf{B}_b^T)\boldsymbol{\sigma}_e^n + \mathbf{B}_s^T\boldsymbol{\tau}_e^n]dV_e \tag{20}$$

where the stress increments are computed from Eq. (6) and the strain increments are $\Delta\boldsymbol{\varepsilon}_t = \boldsymbol{\alpha}\Delta T$ and $\Delta\boldsymbol{\varepsilon}_c = \boldsymbol{\beta}\Delta X$.

All the terms relating to $\Delta\boldsymbol{\sigma}_e^{n+1}$, $\Delta\boldsymbol{\tau}_e^{n+1}$ in the left-hand side of Eq. (20) must be computed at the Gaussian stations used in the numerical integration. The constitutive tensor is the rubbery modulus tensor $\mathbf{C}_r$ or the glassy modulus tensor $\mathbf{C}_g$, depending on T relative to T_{gel}. The same holds for the coefficients $\boldsymbol{\alpha}$ and $\boldsymbol{\beta}$.

At this juncture it is convenient to adapt Eq. (6) to the grouping of stresses presented in Eqs. (14) and (15). Equation (6) can then be split in two:

$$\Delta\boldsymbol{\sigma}_e = \begin{cases} \mathbf{Q}_r\Delta(\boldsymbol{\varepsilon}_0 + z\boldsymbol{\kappa} - \boldsymbol{\varepsilon}_t - \boldsymbol{\varepsilon}_c) - \mathbf{s}_{\sigma\varepsilon} & , \quad T \geq T_g(X) \\ \mathbf{Q}_g\Delta(\boldsymbol{\varepsilon}_0 + z\boldsymbol{\kappa} - \boldsymbol{\varepsilon}_t - \boldsymbol{\varepsilon}_c) & , \quad T < T_g(X) \end{cases}, \quad \Delta\boldsymbol{\tau}_e = \begin{cases} \mathbf{Q}_{sr}\Delta\boldsymbol{\gamma} - \mathbf{s}_{\tau\varepsilon} & , \quad T \geq T_g(X) \\ \mathbf{Q}_{sg}\Delta\boldsymbol{\gamma} & , \quad T < T_g(X) \end{cases} \tag{21}$$

where the constitutive tensor, either in the rubbery or glassy state, has also been split in two. One part relates to the in-plane stresses and strains ($\mathbf{Q}$), whereas the other part relates to transverse shear stresses and strains ($\mathbf{Q}_s$). It is tacitly assumed in Eq. (21) that the thermal and chemical strains do not depend on z and also that they do not influence the transverse shear stresses and strains.

Substitution of Eq. (21) into (20),

$$\sum_{e=1}^{N_e}\int_{V_e}(\mathbf{B}_m^T+z\mathbf{B}_b^T)[\mathbf{Q}\Delta(\boldsymbol{\varepsilon}_0^{n+1}+z\boldsymbol{\kappa}^{n+1}-\boldsymbol{\varepsilon}_t^{n+1}-\boldsymbol{\varepsilon}_c^{n+1})-\mathbf{s}_{\sigma\varepsilon}^{n+1}]dV_e+\sum_{e=1}^{N_e}\int_{V_e}\mathbf{B}_s^T(\mathbf{Q}_s\Delta\boldsymbol{\gamma}^{n+1}-\mathbf{s}_{\tau e}^{n+1})dV_e= \tag{22}$$
$$\mathbf{f}_{ext}^{n+1}-\sum_{e=1}^{N_e}\int_{V_e}[(\mathbf{B}_m^T+z\mathbf{B}_b^T)\boldsymbol{\sigma}_e^n+\mathbf{B}_s^T\boldsymbol{\tau}_e^n]dV_e$$

where it must be clear that $\mathbf{Q}$ and $\mathbf{Q}_s$ assume different values depending on whether $T \geq T_g(X)$ or not as determined by Eq. (21). Moreover, if $T < T_g(X)$, then $\mathbf{s}_{\sigma e} = \mathbf{0}$ and $\mathbf{s}_{\tau e} = \mathbf{0}$.

It is clear from Eq. (9) that the strains, and therefore their increments, depend linearly on the through the thickness variable z. Hence, Eq. (7) also leads to the conclusion that $\mathbf{s}_{\sigma e}$ depend linearly on z. It means that $\mathbf{s}_{\sigma e}$ can be further split into two parts such that

$$\mathbf{s}_{\sigma e}=\mathbf{s}_{\sigma\varepsilon e}+z\mathbf{s}_{\sigma\kappa e} \tag{23}$$

where $\mathbf{s}_{\sigma\varepsilon e}$ can be interpreted as the state variables on the element mid surface and $\mathbf{s}_{\sigma\kappa e}$ have to do with its variation along the thickness. Notice that $\mathbf{s}_{\tau e}$ does not depend on z.

The strain relations in Eq. (13) and Eq. (23) can now be substituted into Eq. (22) leading to

$$\sum_{e=1}^{N_e}\int_{V_e}(\mathbf{B}_m^T+z\mathbf{B}_b^T)\mathbf{Q}\Delta(\boldsymbol{\varepsilon}_0^{n+1}+z\boldsymbol{\kappa}^{n+1})dV_e+\sum_{e=1}^{N_e}\int_{V_e}\mathbf{B}_s^T\mathbf{Q}_s\Delta\boldsymbol{\gamma}^{n+1}dV_e= \tag{24}$$
$$\mathbf{f}_{ext}^{n+1}-\sum_{e=1}^{N_e}\int_{V_e}[(\mathbf{B}_m^T+z\mathbf{B}_b^T)\boldsymbol{\sigma}_e^n+\mathbf{B}_s^T\boldsymbol{\tau}_e^n]dV_e+\sum_{e=1}^{N_e}\int_{V_e}(\mathbf{B}_m^T+z\mathbf{B}_b^T)[\mathbf{Q}\Delta(\boldsymbol{\varepsilon}_t^{n+1}+\boldsymbol{\varepsilon}_c^{n+1})+\mathbf{s}_{\sigma e}^{n+1}]dV_e+\sum_{e=1}^{N_e}\int_{V_e}\mathbf{B}_s^T\mathbf{s}_{\tau e}^{n+1}dV_e$$

It can be seen that Eq. (24) may be restated as

$$\sum_{e=1}^{N_e}\mathbf{K}_e\Delta\mathbf{q}_e=\mathbf{f}_{ext}^{n+1}-\mathbf{f}_{\text{int}}^n+\Delta\mathbf{f}_t+\Delta\mathbf{f}_c+\Delta\mathbf{f}_s \tag{25}$$

where

$$\mathbf{K}_e=\int_{V_e}[(\mathbf{B}_m^T+z\mathbf{B}_b^T)\mathbf{Q}(\mathbf{B}_m+z\mathbf{B}_b)+\mathbf{B}_s^T\mathbf{Q}_s\mathbf{B}_s]dV_e \tag{26}$$

$$\mathbf{f}_{\text{int}}^n=\sum_{e=1}^{N_e}\int_{V_e}[(\mathbf{B}_m^T+z\mathbf{B}_b^T)\boldsymbol{\sigma}_e^n+\mathbf{B}_s^T\boldsymbol{\tau}_e^n]dV_e$$

$$\Delta\mathbf{f}_t=\sum_{e=1}^{N_e}\int_{V_e}(\mathbf{B}_m^T+z\mathbf{B}_b^T)\mathbf{Q}\Delta\boldsymbol{\varepsilon}_t^{n+1}dV_e=\sum_{e=1}^{N_e}\int_{V_e}(\mathbf{B}_m^T+z\mathbf{B}_b^T)\mathbf{Q}\boldsymbol{\alpha}\Delta T dV_e$$

$$\Delta\mathbf{f}_c=\sum_{e=1}^{N_e}\int_{V_e}(\mathbf{B}_m^T+z\mathbf{B}_b^T)\mathbf{Q}\Delta\boldsymbol{\varepsilon}_c^{n+1}dV_e=\sum_{e=1}^{N_e}\int_{V_e}(\mathbf{B}_m^T+z\mathbf{B}_b^T)\mathbf{Q}\boldsymbol{\beta}\Delta X dV_e$$

$$\Delta\mathbf{f}_s=\sum_{e=1}^{N_e}\int_{V_e}(\mathbf{B}_m^T+z\mathbf{B}_b^T)\mathbf{Q}(\mathbf{s}_{\sigma\varepsilon e}^{n+1}+z\mathbf{s}_{\sigma\kappa e}^{n+1})dV_e+\sum_{e=1}^{N_e}\int_{V_e}\mathbf{B}_s^T\mathbf{Q}_s\mathbf{s}_{\tau e}^{n+1}dV_e$$

Notice that the dependency on variable z is explicit in Eq. (26). Therefore, it is possible to carry out integration along z analytically. It all depends on the constitutive matrices. In

isotropic materials **Q** and $\mathbf{Q}_s$ are constant. However, if laminates are considered, then these matrices are piecewise constant. On the other hand, the integration in the x and y variables must be done numerically through Gaussian quadrature. The term containing **Q** in $\mathbf{K}_e$ is fully integrated. However, reduced integration is used to integrate the term containing $\mathbf{Q}_s$ in $\mathbf{K}_e$.

Equation (25) is used to find the displacement increments. Observe that, if T, X, the mechanical loading and the state variables at step n are known, then $\Delta\mathbf{q}$ can be computed. If the problem is geometrically linear Eq. (25) has to be solved only once at each time step.

NUMERICAL EXAMPLES

Two simple numerical examples involving bars will be used to validate the code developed. In both examples the bars are assumed to be made purely out of resin. The objective of these simulations is to study how thermal and chemical stresses develop. A bar with length L = 1.0 m, width W = 0.1 m and 0.01 m thickness is modeled using 10 identical 4-noded plate elements.

The mechanical properties adopted in the rubbery and glassy states are in Tab. 1.

Table 1: Mechanical properties

state	E (GPa)	ν	G (GPa)	α ($^{o}C^{-1}$)
glassy	2.6	0.38	0.94	71.0×10^{-6}
rubbery	0.028	0.497	0.0094	177.5×10^{-6}

Additional properties are: coefficient of chemical shrinkage (β = –0.02333), fully cured glass transition temperature ($T_{g\infty}$ = 136 ^{o}C), uncured glass transition temperature (T_{g0} = –41 ^{o}C), degree of cure at gelation (X_{gel} = 0.5)and material constant in Eq. (4) (λ = 0.44).

Test case 1

Figure 1 shows the bar that has one end fully restrained (clamped) and the other end subjected to a mechanical stress σ. Mechanical load and temperature vary according to Fig. 3, while the degree of cure is constant (X = 1).

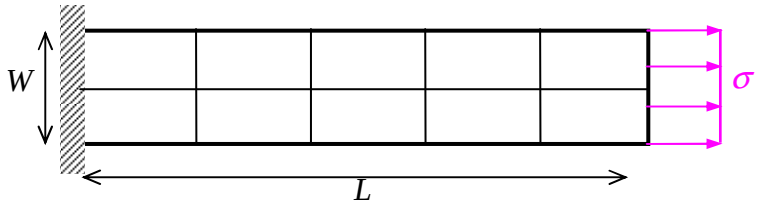

Figure 2: Mesh, loading and boundary conditions for test case 1.

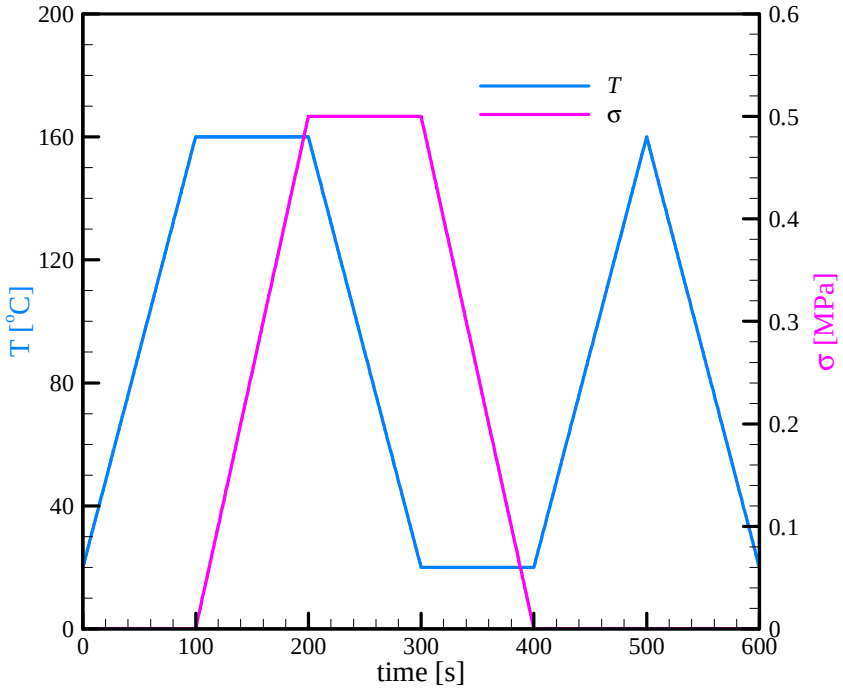

Figure 3: Temperature and mechanical loading history for test case 1.

The results obtained in terms of strains (%) are in Fig. 4, where the expansion strain coincides with the thermal strain in this simulation since there are no chemical shrinkage strains ($\Delta X = 0$). This result is in full accordance with those obtained by Svanberg and Holmberg (Svanberg *et al.* 2001, 2004a, 2004b). Minimal differences may be perceived since there is a small Poison effect in the present model that was not included in Svanberg's calculations.

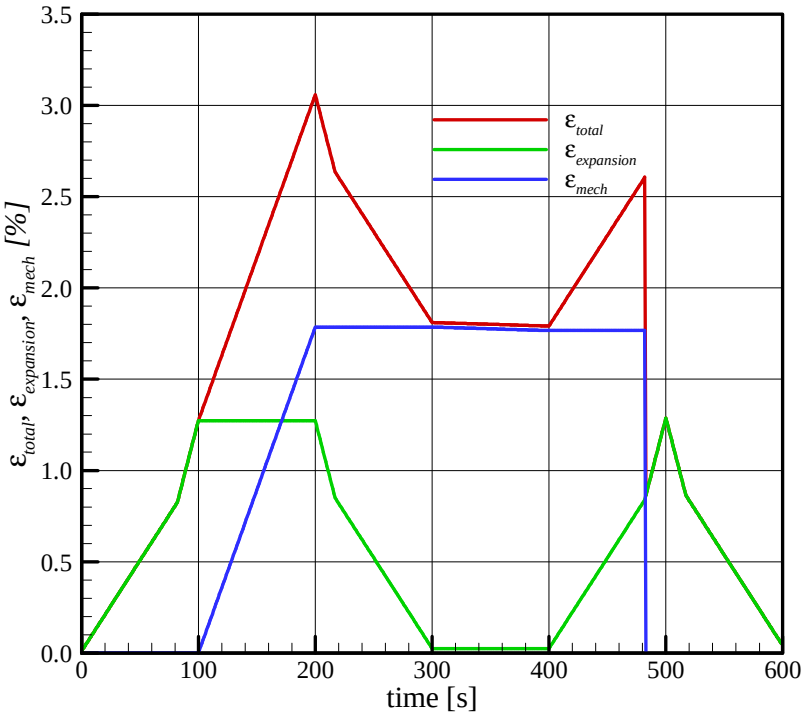

Figure 4: Strains in test case 1.

Test case 2

Figure 5 shows the bar that has initially both ends fully restrained (clamped) up to time t = 150 s. After 150 s one end of the bar is released. Temperature and degree of cure vary according to Fig. 6. This example simulates demoulding since, before t = 150 s, the bar is assumed to be completely restrained (in mould) under cure. After cure at 120 ^{o}C is complete the specimen cools down to 20 ^{o}C. At t = 150 s demoulding happens and the stress drops to zero as shown in Fig. 7 whereas a nonzero total strain appears as illustrated in Fig. 8.

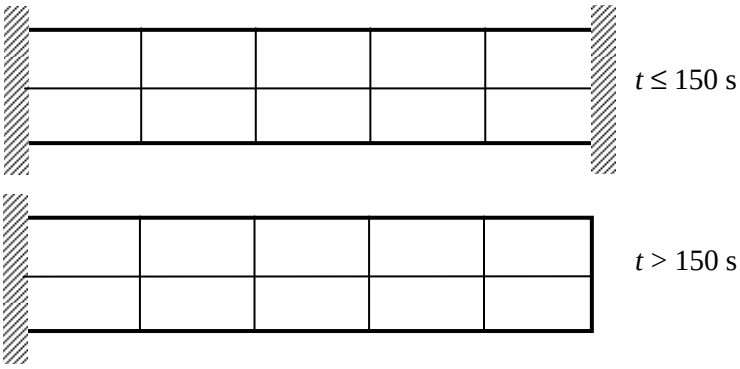

Figure 5: Mesh, loading and boundary conditions for test case 2.

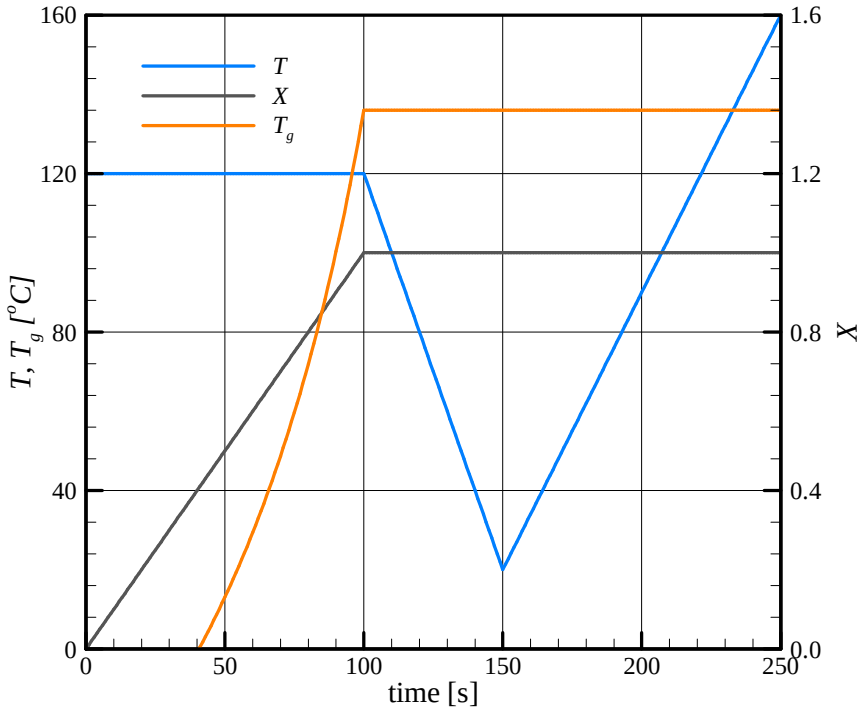

Figure 6: Temperature and mechanical loading history for test case 2.

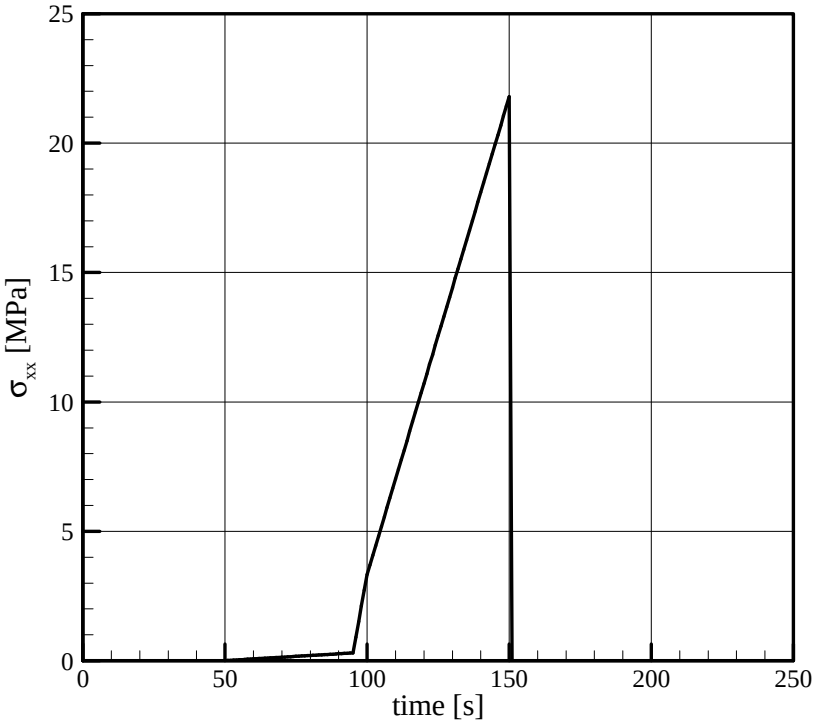

Figure 7: Stress in test case 2.

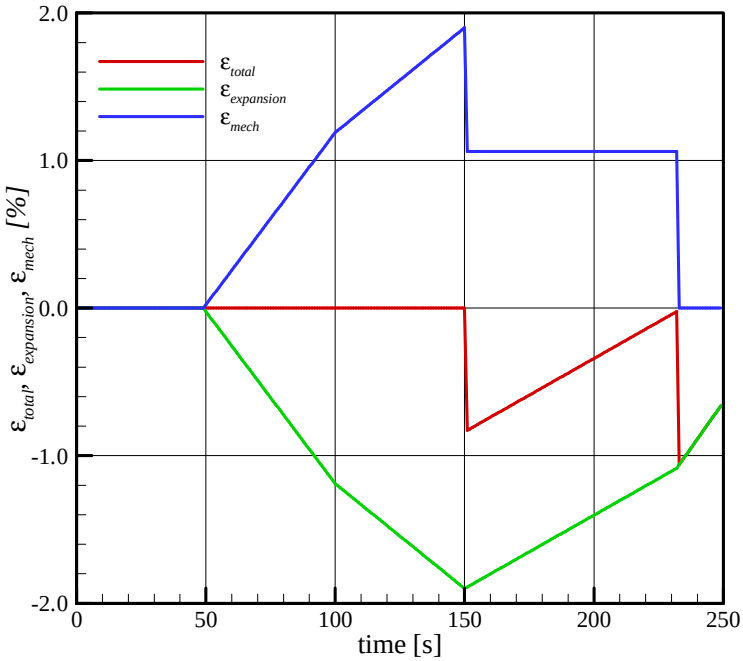

Figure 8: Strains in test case 2.

After t = 150 s the specimen is again heated up until it reaches 160 ^{o}C. Since the glass transition temperature is 136 ^{o}C, frozen strains are released as can be observed in the sudden drop of total strains at around t = 233 s as shown in Fig. 8.

CONCLUSIONS

This work shows that a simple constitutive model is capable of capturing the most relevant aspects of real cure processes. Most important, demoulding and residual strains/stresses can be studies from a numerical perspective.

In the next phases of this project fiber reinforced plies shall be considered. In order to obtain the homogenized elastic properties of the ply a micromechanical model shall be developed that depends on the volume fraction of fibers and considers that the resin constitutive relations are governed by Eqs. (1)-(7) presented in this paper.

ACKNOWLEDGEMENTS

This work was partially funded by CISB through grants related to Calls of Innovation Projects 02/2015 (Senior Internship Abroad) and 03/2016 (Program to support events in Sweden), and the Brazilian Agency CNPq through grant 300886/2013-6.

REFERENCES

Almeida, S.F.M. & Hansen, J.S. 1999 Natural frequencies of composite plates with tailored thermal residual stresses. *International Journal of Solids and Structures*, **36**, 3517-3539.

Cho, M., Kim, M.H., Choi, H.S., Chung, C.H., Ahn, K-.J. & Eom, Y.S. 1998 A study on the room temperature curvature shapes of unsymmetric laminates including slippage effects. *Journal of Composite Materials*, **32**, 460-483.

Faria, A.R. & Hansen, J.S. 1999 Optimal buckling loads of nonuniform composite plates with thermal residual stresses. *Journal of Applied Mechanics*, **66**, 388-395.

Holmberg, J.A. 1998 Influence of chemical shrinkage on shape distortion of RTM composites. *Proceedings of the 19th International SAMPE European Conference of the Society for the Advancement of Material and Process Engineering*, Paris, France.

Hull, D. 1998 *An Introduction to Composite Materials*. Cambridge University Press.

Kaw, A.K. 2006 *Mechanics of Composite Materials*. CRC Taylor & Francis, second ed., Boca Raton.

Kenny, J.M., Maffezoli, A., Nocolais, L. & Mozzola, M.S.A. 1990 A model for the thermal and chemorheological bahavious of thermoset processing: (II) unsaturated polyester based composites. *Composites Science and Technology*, **38,** 339-358.

Kenny, J.M. 1992 Integration of processing models with control and optimization of polymer composite fabrication, *Computer Aided Design in Composite Material Technology III*, 529-544.

Kim, K.K. & White, S.S. 1997 Viscoelastic analysis of processing-induced residual stresses in thickn composite laminates. *Mechanics of Composite Materials and Structures*, **4**, 361-387.

Radford, D.W. & Rennick, T.S. 1997 Determination of manufacturing distortion in laminated composite components. *Proceedings of ICCM-11*, Gold Coast, Australia.

Kolkman, J. 1974 Testing epoxide castings by thermal analysis. *Holectecniek*, **4**, 29-35.

Lundström, T.S., Gebart, B.R. & Lundemo, C.Y. 1993 Void formation in RTM. *Journal of Reinforced Plastics and Composites*, **12**, 1340-1349.

Sarrazin, H., Beomkeum, K., Ahn, S.-H. & Springer, G.S. 1995 Effects of the processing temperature and lay-up in springback. *Journal of Composite Materials*, **29**, 1278-1294.

Svanberg, J.M. & Holmberg, J.A. 2001 An experimental investigation on mechanisms for manufacturing induced shape distortions in homogeneous and balanced laminates. *Composites Part A*, **32**, 827-838.

Svanberg, J.M. & Holmberg, J.A. 2004 Prediction of shape distortions Part I. FE-implementation of a path dependent constitutive model. *Composites Part A*, **35**, 711-721.

Svanberg, J.M. & Holmberg, J.A. 2004 Prediction of shape distortions Part II. Experimental validation and analysis of boundary conditions. *Composites Part A*, **35**, 723-734.

White, S.R. & Hahn, H.T. 1993 Cure cycle optimization for the reduction of processing induced residual stresses in composite materials. *Journal of Composite Materials*, **27**, 1352-1378.